JOURNAL OF MOLECULAR SPECTROSCOPY **146**, 465–492 (1991)

Rotational Analysis of the BaI $C^2\Pi$–$X^2\Sigma^+$ (8,8) Band

CHRISTINE A. LEACH, JANET R. WALDECK,[1] CHIFURU NODA,[2]
JOHN S. MCKILLOP,[3] AND RICHARD N. ZARE

Department of Chemistry, Stanford University, Stanford, California 94305

The BaI $C^2\Pi$–$X^2\Sigma^+$ (8,8) band has been measured and rotationally assigned using techniques of population-labeling optical–optical double resonance (PLOODR) and selectively detected laser-induced fluorescence (SDLIF). A weighted nonlinear least-squares fit has been carried out to model the positions of 891 transitions with J'' ranging from 13.5 to 271.5, to a $^2\Pi$–$^2\Sigma^+$ Hamiltonian which has 10 spectroscopic constants. Despite the fact that most of our data is from 6 out of the possible 12 rotational branches and is biased in favor of the $C^2\Pi_{1/2}$–$X^2\Sigma^+$ subband, we are able to assign J'' quantum numbers unambiguously for all the observed transitions as well as derive the principal spectroscopic constants of the BaI $C^2\Pi$ and $X^2\Sigma^+$ states for the (8,8) band.

1. INTRODUCTION

The $C^2\Pi$–$X^2\Sigma^+$ band system of the diatomic molecule BaI is centered at approximately 550 nm and is divided into two well-separated subbands by a large spin–orbit interaction (780 cm^{-1}) in the $C^2\Pi$ state. Although there have been a number of spectroscopic studies of this molecule (*1–12*), including a rotational analysis of the (0,0) vibrational band (*1*), a complete rovibrational analysis of this system is still to be carried out. In this paper we describe the rotational analysis of the (8,8) band. This particular vibrational transition was chosen because the $X^2\Sigma^+ v'' = 8$ level has significant population both from a thermal oven source and from the Ba + HI reaction (*13*). The incentive to carry out this analysis was to provide a rotational assignment for the study of the dynamics of the reaction Ba + HI → BaI ($v'' = 8$) + H (*13*).

The BaI molecule was first identified in 1927 in an absorption spectrum recorded by Walters and Barratt (*2*). They observed bands from the $C^2\Pi$–$X^2\Sigma^+$ transition and also noticed some absorption in the region of 380 nm. Later, Mesnage studied the bandheads[4] of the two $C^2\Pi$–$X^2\Sigma^+$ subbands, the $C^2\Pi_{3/2}$–$X^2\Sigma^+$ at 538.3 nm and the $C^2\Pi_{1/2}$–$X^2\Sigma^+$ at 561.2 nm (*3*). Patel and Shah analyzed the bandheads in the $C^2\Pi$–$X^2\Sigma^+$ transition (*4*), and also recognized that the absorption in the region of 380 nm observed by Walters and Barratt (*2*) was caused by two other electronic band systems, the $E^2\Sigma^+$–$X^2\Sigma^+$ transition at about 374 nm and the $D^2\Sigma^+$–$X^2\Sigma^+$ transition at about

[1] Present address: Chemistry Department, University of Pittsburgh, Pittsburgh, PA 15260.

[2] Present address: Department of Chemistry, University of New Hampshire, Durham, NH 03824.

[3] Present address: American Laser Corporation, 1832 South 3850 West, Salt Lake City, UT 84104.

[4] Work in this laboratory shows that the bandheads in BaI are not formed for $J'' < 420.5$ (*14*); these earlier studies actually observed closely spaced lines corresponding to points of inflection on a Fortrat diagram. However, we follow the earlier nomenclature and refer to them as bandheads.

0022-2852/91 $3.00

388 nm (*4*). Bradford *et al.* studied chemiluminescence of BaI formed by the reaction of Ba with I_2 (*5*). They observed emission in the infrared which they determined to be caused by two previously unobserved electronic transitions, the $A^2\Pi$–$X^2\Sigma^+$ and the $B^2\Sigma^+$–$X^2\Sigma^+$ (*5*). Recently Fernando *et al.* observed the $A'\,^2\Delta$ state, which is the lowest known excited state, by using a high-resolution infrared Fourier transform spectrometer to resolve the laser-induced fluorescence from the $C^2\Pi$ state to the $A'\,^2\Delta$ state (*6*).

Improved vibrational constants for the $C^2\Pi$ and $X^2\Sigma^+$ states were obtained by Rao *et al.* (*7*) and a comprehensive study of the bandheads in the $C^2\Pi$–$X^2\Sigma^+$, $D^2\Sigma^+$–$X^2\Sigma^+$, and $E^2\Sigma^+$–$X^2\Sigma^+$ systems has been carried out by Patel (*8*). These studies of the vibrational structure of the $C^2\Pi$–$X^2\Sigma^+$ transition show that in both subbands the vibrational bandheads are separated by about 6 cm^{-1} and that for low values of v'' the spectrum is dominated by the $\Delta v = 0$ sequence, which has Franck–Condon factors close to unity. Analysis of transitions involving higher vibrational levels has been carried out by Johnson *et al.* using BaI molecules produced by various gas-phase reactions (*9*). High vibrational levels in the $C^2\Pi$ state were shown to predissociate ($v' > 62$ for $C^2\Pi_{3/2}$ and $v' > 78$ for $C^2\Pi_{1/2}$).

The $C^2\Pi$–$X^2\Sigma^+$ spectrum has very closely spaced rotational lines (<0.1 cm^{-1} separation) and overlapping vibrational bands which make a comprehensive measurement of a rotationally resolved spectrum very difficult. This is a consequence of two factors: first the reduced mass of the molecule means BaI has a small rotational constant ($B'' \approx 0.026$ cm^{-1}) causing many levels to be populated under thermal conditions, and second the nature of the $C^2\Pi$–$X^2\Sigma^+$ transition. The electron that is excited in this transition moves between two nonbonding orbitals, both of which are situated mainly on the Ba atom (*15*). This results in almost identical potential energy curves for the $C^2\Pi$ and $X^2\Sigma^+$ electronic states, both in equilibrium bond length and in shape. The absence of $\Delta v = \pm 1$ transitions for low v'' ($v'' < 10$) provides evidence that the shape close to the bottom of the two potential wells is nearly identical. A consequence of this is that the vibrational constants of the two electronic states are also very similar and vibrational bands are only separated by about 6 cm^{-1}. In addition each vibrational subband is divided into six rotational branches. Thus there is considerable overlap both between the different vibrational bands and between different rotational branches within one vibrational band. The rotational analysis of the $C^2\Pi$–$X^2\Sigma^+$ transition therefore requires the use of narrow-band lasers and special techniques to obtain sub-Doppler resolution.

To illustrate this problem, we estimate the number of lines in the region of the (8,8) band origin to be about 250 per cm^{-1} for a thermal population of BaI at the temperature of the oven source (1300 K). This number does not take account of the hyperfine structure arising from the ^{127}I nucleus ($I = 5/2$) which would cause each rotational line to split into six hyperfine components. (The major isotope of Ba has no nuclear spin.) The hyperfine structure of the BaI $X^2\Sigma^+$ and $C^2\Pi$ states has been studied in detail by Ernst *et al.* (*10*) and its influence on the analysis of the (8,8) band is discussed below.

The $C^2\Pi$ state of BaI is an example of a Hund's case (a) coupling (*16*) since the spin–orbit constant, A', is greater than the rotational constant, B', by a factor of 3×10^4. With the Λ doubling of the $^2\Pi$ state and spin–rotation splitting of the $^2\Sigma^+$

ground state, each vibrational band in the electronic spectrum consists of two well-separated subbands that have six rotational branches (*16*). The assignment of the branches would be very difficult by traditional combination relation techniques (*16*). To overcome this problem Johnson and Zare (*11*) used the technique of population-labeling optical–optical double resonance (PLOODR) to assign the $C^2\Pi$–$X^2\Sigma^+$ (0,0) band. The same approach was used for the (8,8) band.

To measure the spectrum of one rotational branch without interference from others that overlap in the same wavelength region, the technique of selectively detected laser-induced fluorescence (SDLIF) was used. This method was first introduced in 1978 by Linton (*17*) to study the $A^2\Pi$–$X^2\Sigma^+$ system of yttrium oxide, YO. It was subsequently used by Dulick *et al.* (*18*). Once an assignment has been obtained using PLOODR, SDLIF can be used to measure the frequencies of up to several hundred lines in a branch. This approach was also employed in measuring the BaI $C^2\Pi$–$X^2\Sigma^+$ (0,0) band (*1*).

2. EXPERIMENTAL DETAILS

Details of the techniques and apparatus used in this study have been described elsewhere (*1, 11*). A summary of the two methods, population-labeling optical–optical double resonance and selectively detected laser-induced fluorescence, follows.

(a) Population-Labeling Optical–Optical Double Resonance (PLOODR)

The energy level diagram in Fig. 1 demonstrates the principles involved in PLOODR. The technique uses two dye lasers, both tuned to the rotational structure of the vibronic transition being analyzed. The frequency of one laser, the probe laser, is fixed at the frequency of a single rotational transition. By constantly monitoring the laser-induced fluorescence (LIF) excited by this laser, the population of the ground state rotational level, the "labeled" level, is recorded. The second laser, the pump laser, is scanned across the entire rotational spectrum of the vibronic transition being studied. This laser must be powerful enough to reduce the population of the ground state levels as it excites the transitions. The large separation between the two subbands allows one laser to excite each subband and the resulting LIF from each laser to be collected independently using broad-band spectral filters. When the pump laser induces a transition originating from the labeled level, a decrease in the population of this state is observed. On the other hand, when this laser excites molecules to an upper state that fluoresces to the labeled ground state, the population increases. This is observed as an increase in the fluorescence signal intensity. In a band of the $C^2\Pi$–$X^2\Sigma^+$ system there are a total of nine possible PLOODR signals for each labeled rotational level, of which six are positive and three are negative. This is illustrated in Fig. 1.

An assignment of the rotational numbering can be established and the parity of the ground state and the sign of the spin–rotation constant of the $X^2\Sigma^+$ can be determined by comparing the PLOODR patterns with simulations based on estimated constants and measuring the spacings between the signals (*11*).

(b) Selectively Detected Laser-Induced Fluorescence (SDLIF)

In SDLIF a single scanning laser is used to excite molecules and the resulting fluorescence is detected with a narrow-band filter whose transmission is fixed at a different

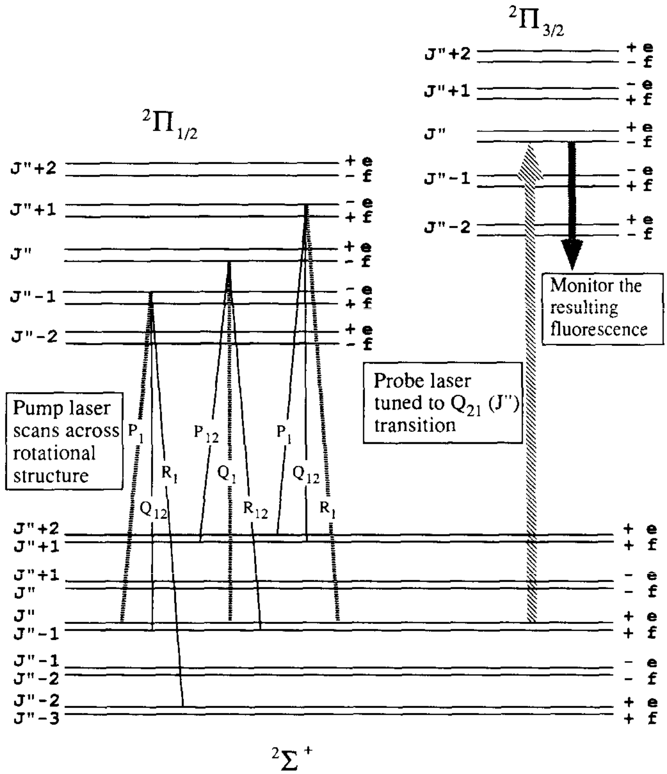

FIG. 1. Energy level diagram illustrating the principles of PLOODR as applied to the BaI $C^2\Pi$–$X^2\Sigma^+$ transition. As the pump laser is scanned, nine double resonance signals are expected, three as a decrease in fluorescence (broken lines labeled P_1, Q_1, R_1) and six as an increase (solid lines labeled Q_{12}, R_1, P_{12}, R_{12}, P_1, Q_{12}).

wavelength from the excitation laser. The detector wavelength "window" is chosen so that it collects fluorescence from transitions that have a common upper level with those being excited. Ideally the detector window should be set close to a bandhead so that many rotational lines can be scanned without changing the wavelength of the detector. However this is not essential and measurement of the Q-branch members was carried out by gradually altering the detector wavelength (between scans) along the appropriate P or R branch. An illustration of the SDLIF technique as applied to the measurement of the P_2 branch is given in the upper panel of Fig. 2. The detector window is set to collect the Q_{21}- and R_2-branch members that have a J'' between about 50.5 and 300.5; the laser is scanned along the P_2-branch transitions.

(c) Procedure

In all the experiments a molecular beam of BaI was produced by heating Ba and BaI_2 in a stainless steel crucible to approximately 1300 K. The beam was subsequently collimated to reduce the Doppler width to about 120 MHz when excited by a laser beam perpendicular to the molecular beam.

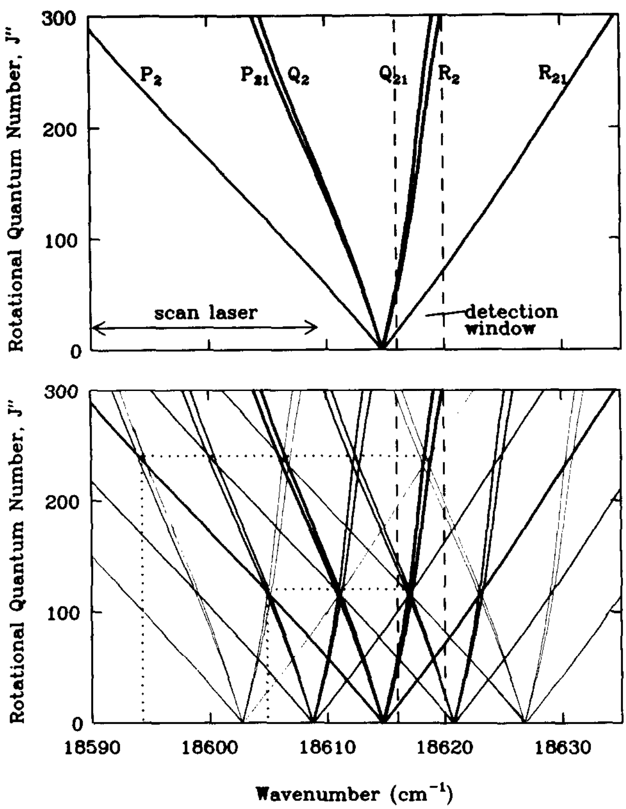

FIG. 2. Fortrat diagram (upper panel) of the BaI $C^2\Pi_{3/2}$–$X^2\Sigma^+$ (8,8) subband illustrating selective detection of the P_2 branch. The lower panel shows the same Fortrat diagram as the upper panel except that all vibrational bands from (6,6) to (10,10) are included to demonstrate how complicated the picture becomes when other vibrational bands are considered. The dotted lines show where two areas of contamination from other bands are expected as the P_2-branch spectrum is scanned.

For the PLOODR experiment two single-mode continuous-wave lasers were used, a Coherent 599-21 linear dye laser and a Spectra-Physics 380D ring dye laser. Both were pumped by a Spectra-Physics 171-17 argon ion laser, which gave about 6 W at 514.5 nm. For the region of the spectrum where the BaI $C^2\Pi$–$X^2\Sigma^+$ band system is located, the dye rhodamine 560 was used. A power of about 50 mW was used in each subband for double resonance spectra. The fluorescence from the BaI beam was collected at $f/3$ and divided into two paths by a 50% beam splitter. Each fluorescence beam was then detected by a photomultiplier with the appropriate filter to isolate the fluorescence from one spin–orbit subband. The pump laser was chopped so that lock-in detection could be used. The double resonance spectrum was obtained using a lock-in amplifier to monitor the probe beam fluorescence at the modulation frequency of the pump beam. An iodine spectrum and the fringes of a 250 MHz etalon were recorded simultaneously with each PLOODR spectrum. Absolute frequency calibration was performed by interpolating between the frequencies of iodine reference lines (*19*) using the etalon fringes.

For the SDLIF experiments only one dye laser was required. Data for the $C^2\Pi_{1/2}$–$X^2\Sigma^+$ subband were collected using the Coherent 599-21 laser while data for the $C^2\Pi_{3/2}$–$X^2\Sigma^+$ were collected using a Coherent 699-29 ring dye laser because it gave more power in this region of the spectrum. Rhodamine 560 dye was used for both subbands but a few drops of a buffered base were added to the dye solution to shift the dye fluorescence profile to the shorter wavelengths required for $C^2\Pi_{3/2}$–$X^2\Sigma^+$. A 1-m monochromator (Interactive Technology CT103) was used to disperse the fluorescence. The entrance and exit slits could be varied between 0 and 3 mm. Usually 150-μm slits were used, which gave a band-pass width of between 3 and 4 cm^{-1}. The dispersed fluorescence was measured by single-photon counting; the signal from the photomultiplier (Centronic Q4283 RA) was amplified (Ortec 9301/474) and converted to an analog signal by a discriminator/ratemeter combination (Ortec 436 and 449). With this arrangement count rates on resonance were on the order of 300 counts s^{-1}. For absolute frequency calibration an I_2 spectrum and the fringes of a 250 MHz etalon were recorded simultaneously for each SDLIF scan.

3. RESULTS AND ANALYSIS

The PLOODR procedure was repeated for a number of different rotational transitions in the $C^2\Pi_{1/2}$–$X^2\Sigma^+$ subband and for one transition in $C^2\Pi_{3/2}$–$X^2\Sigma^+$. A total of 25 PLOODR transitions were assigned. Figure 3 shows a PLOODR spectrum from the BaI $C^2\Pi_{3/2}$–$X^2\Sigma^+$ (8,8) subband and the I_2 spectrum with superimposed etalon fringes which was recorded simultaneously. By comparing the observed pattern with

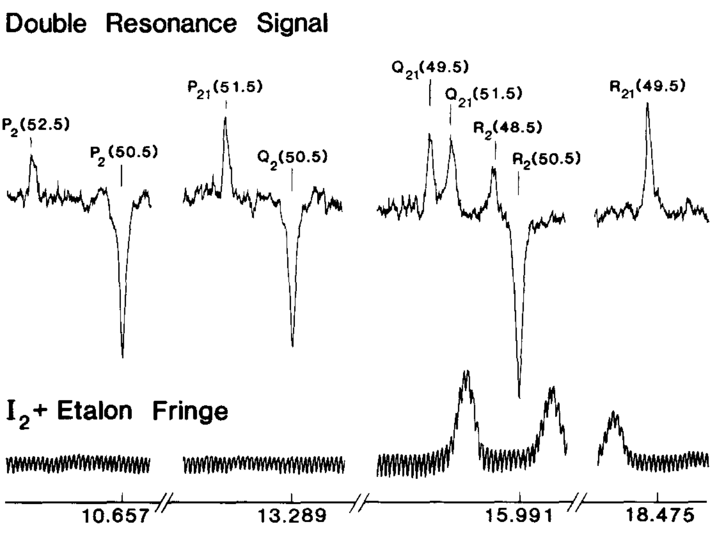

FIG. 3. An example of a PLOODR spectrum for the BaI $C^2\Pi_{3/2}$–$X^2\Sigma^+$ (8,8) in which the probe laser was tuned to label the ground state $J'' = 50.5$ level while the pump laser was scanned across the rotational structure of the transition. The I_2 spectrum with superimposed etalon fringes is shown in the lower panel, which was recorded simultaneously for wavenumber calibration.

hypothetical calculated patterns (*11*) the parity of the ground state rotational level was determined to be *f* and the sign of the ground state spin-rotational constant, γ'', to be positive. The J'' assignment was carried out using simplified energy level expressions for the two states (only B', B'', and γ'' were used). Estimates of the B constants were used to calculate the value of J'' from various combination relations of the measured lines. For the spectrum illustrated in Fig. 3 the J'' was found to be 50.5.

Figure 4 shows an example of a SDLIF spectrum for the P_2 branch. The monochromator was tuned to the (Q_{21}, R_2) branches to collect this data [see Fig. 2 (upper panel)]. The parentheses around (Q_{21}, R_2) are used to denote a pair of very closely spaced branches. The I_2 spectrum, which was used for absolute calibration, is also shown. The lower panel of Fig. 2 illustrates how the application of SDLIF to this level is not completely straightforward. When the monochromator is tuned to the (8,8) (Q_{21}, R_2) branches a portion of the (7,7) R_{21}-branch members can also be detected. This causes the excitation of the (7,7) (Q_2, P_{21}) transitions ($J'' \approx 120.5$) to be observed in one part of the (8,8) P_2 SDLIF spectrum ($J'' \approx 120.5$). The lower panel of Fig. 2 also shows where contamination of the P_2 branch will occur from the (6,6) vibrational band. The beginning of this overlap is visible in the spectrum in Fig. 4; at the low wavenumber end where the baseline rises, there are underlying (Q_2, P_{21})-branch members of the (6,6) band which are not resolved. Similar problems arise for the other branches; for example, R_{21} is contaminated by the (Q_{21}, R_2) branches of the (9,9) band in the region of $J'' \approx 120.5$.

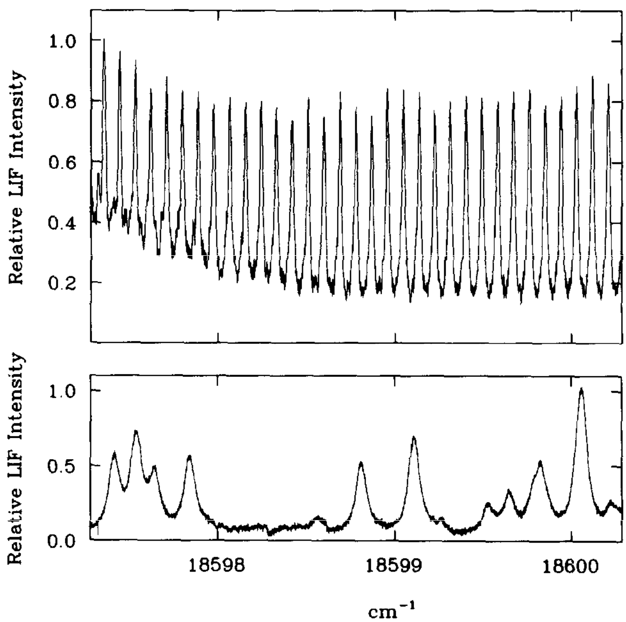

FIG. 4. The upper panel shows a portion of the P_2 branch from the BaI $C^2\Pi_{3/2}$–$X^2\Sigma^+$ (8,8) subband between $J'' = 202.5$ and 170.5 (left to right) recorded using SDLIF (see Fig. 2). The lower panel shows the I_2 spectrum recorded simultaneously for calibration.

From the Fortrat diagram in Fig. 2 (upper panel) it can be seen that the (P_{21}, Q_2) branches lie almost on top of each other. This is the same for the pairs of branches (Q_{21}, R_2), (P_1, Q_{12}), and (Q_1, R_{12}). Each of these pairs of branches involves the same upper level for a particular J''; thus they cannot be separated by selective detection.

In the lower $C^2\Pi_{1/2}$–$X^2\Sigma^+$ subband, the P- and R-branch members are broadened by hyperfine interactions to about 600 MHz compared to 150 MHz for the Q-branch transitions (*10*). This, combined with the dipole moment transition strength of the Q-branch members, which is approximately double that of the P- and R-branch members, means the peak intensity of the Q-branch lines is about five times that of the P- and R-branch lines for the same value of J''. This allowed the measurement of the Q_{12} and Q_1 branches but the weak underlying P_1 and R_{12} branches could not be observed.

In the $C^2\Pi_{3/2}$–$X^2\Sigma^+$ subband the hyperfine splitting for all branches is very similar (about 300 MHz width). The peak intensities of the (P_{21}, Q_2) and (Q_{21}, R_2) transitions are within a factor of 2 of each other. Thus, these branches cannot be easily distinguished. None of these four branches was measured.

A total of 881 different rotational lines were recorded by SDLIF in the P_{12}, Q_1, Q_{12}, R_1, P_{21}, and R_2 branches. (The other 10 lines in the data set were only recorded by PLOODR.) Where assignment of the rotational lines could not be carried out by counting directly up the branch from the PLOODR transitions, extrapolation was used. In most cases, even where a branch was contaminated by transitions in neighboring vibrational bands the overall structure of the branch of interest was dominant and the J'' assignment could still be carried out directly.

The best value of the wavenumber of each recorded rotational line was made by measuring the position of its center of mass. This intensity-weighted mean is chosen to account for hyperfine effects, which result in an asymmetric broadening of the rotational lines (*1*). In the spectra used for this analysis the effects of hyperfine interactions were only just observable in the P_{12} and R_1 branches of the lower subband. An analysis of the hyperfine interactions in BaI $X^2\Sigma^+$ and $C^2\Pi$ states has been carried out and measurement of the center of mass was shown to take account of the asymmetric broadening in the rotational transitions measured (*1*).

Absolute wavenumber calibration for both PLOODR and SDLIF was provided by fitting a polynomial to the peaks of the etalon fringes and then interpolating and extrapolating between the known positions of the iodine lines in each spectrum. In this way the wavenumbers of the transitions measured in the SDLIF spectra are accurate to ± 0.002 cm^{-1} while those measured by PLOODR are accurate to ± 0.005 cm^{-1}. The accuracy of the PLOODR wavenumbers is lower than the SDLIF because the pump and probe laser linewidths were narrower than the BaI rotational linewidths, which are broadened by hyperfine interactions. This could result in a small wavenumber offset in the PLOODR spectra, which is taken into account by the greater uncertainty assigned to these measurements.

The experimental transition wavenumbers were given different weights for fitting because not all the lines measured were known to the same accuracy. As discussed above, the PLOODR data were only good to ± 0.005 cm^{-1} while the best parts of the SDLIF spectra were accurate to ± 0.002 cm^{-1}. In addition a lower weight was used for the SDLIF where there was blending in the spectrum from another branch, when the signal to noise was poor and where hyperfine effects made estimation of the line center more difficult. In addition, when the same transition had been measured more than once, the average wavenumber was used taking appropriate account of the weights, and the weight was adjusted accordingly.

A weighted nonlinear least-squares fit of the measured line positions to the usual $C^2\Pi$–$X^2\Sigma^+$ Hamiltonian was carried out (*20*). First a preliminary fit using nine parameters to the PLOODR wavenumbers and the lower J'' SDLIF data was done. The nine parameters chosen for the fit were the band origin, ν_0, the spin–orbit splitting of the $^2\Pi$ state, A', the lower and upper rotational constants, B'' and B', and their centrifugal distortion corrections, D'' and D', the spin–rotation constant of the ground state, γ'', and the Λ-doubling constants of the upper state, p' and q'. Gradually more rotational lines were included as the assignment was extrapolated up the rotational branches. At each stage the "current best fit" parameters were used to check the new assignments. Particular care had to be taken when there was a gap in the experimental data. For example, only transitions with J'' values greater than 100 were measured for the $C^2\Pi_{3/2}$–$X^2\Sigma^+$ subband so these R_2- and P_{21}-branch members were included in the fit last. The J'' assignments were checked carefully by examining what happened to the overall fit if one branch was reassigned by one unit in J''. In all cases tested, the residuals from the fit showed significant trends so incorrect assignments were easily spotted and discarded.

When all 891 lines had been included with a maximum J'' of 271.5, an investigation was carried out to determine whether all the nine parameters included were needed and whether further centrifugal distortion constants had to be added to reproduce the data within the experimental accuracy. First, the Λ-doubling constant, q', was found to be very poorly determined and a fit without it showed no significant difference

TABLE I

Spectroscopic Constants in cm^{-1} for the BaI $C^2\Pi$–$X^2\Sigma^+$ (8,8) Band Determined from a Weighted Least-Squares Fit of the Data

ν_0	$1.82362071(5) \times 10^4$ [a]
A'	$7.571060(8) \times 10^2$
A_D'	$-4.0(3) \times 10^{-7}$
B'	$2.616285(269) \times 10^{-2}$
D'	$3.0565(178) \times 10^{-9}$
p'	$6.602(7) \times 10^{-3}$
p_D'	$-2.7(2) \times 10^{-9}$
B''	$2.621843(270) \times 10^{-2}$
D''	$3.3130(181) \times 10^{-9}$
γ''	$2.338(10) \times 10^{-3}$

[a] Two standard deviation uncertainties derived from the fit are given in parentheses in units of the last significant figure.

within the experimental error. This constant was therefore omitted from the final fit. Addition of the centrifugal distortion constants, A'_D and p'_D was found to improve the fit significantly whereas addition of the parameters γ''_D, H', and H'' did not.

In total, therefore, 10 adjustable molecular "constants" were included in the least-squares fit. The final values are given in Table I with two-standard-deviation uncertainties derived from the fit. The normalized residuals from the fit are shown in Fig. 5. The upper panel shows those from the $C^2\Pi_{1/2}$–$X^2\Sigma^+$ subband while the lower panel shows those from $C^2\Pi_{3/2}$–$X^2\Sigma^+$. For each transition the normalized residual is the difference between the experimental and calculated wavenumbers (in cm^{-1}) divided by the experimental standard deviation (in cm^{-1}).

The Appendix lists the experimental wavenumbers of the transitions included in the least-squares fit along with wavenumbers calculated using the parameters in Table I, the experimental standard deviations which are equal to the reciprocal of the weights used and the normalized residuals from the fit.

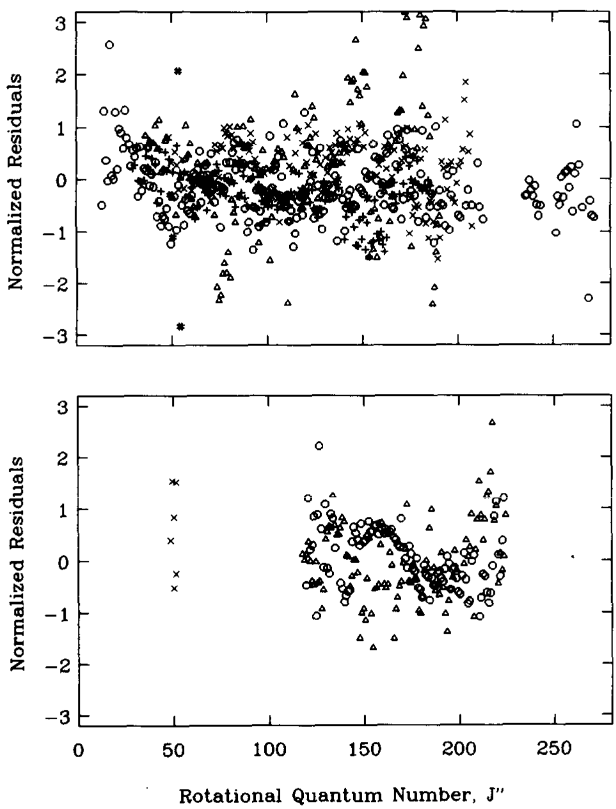

FIG. 5. Residuals from the least-squares fit of the BaI $C^2\Pi_{1/2}$–$X^2\Sigma^+$ (8,8) subband (upper panel; (O) = Q_1, (+) = Q_{12}, (×) = R_1, (△) = P_{12}, and (#) = R_{12} and P_1) and the $C^2\Pi_{3/2}$–$X^2\Sigma^+$ subband (lower panel; (O) = P_2, (△) = R_{21}, (×) = P_{21}, R_2, Q_2, and Q_{21}). The normalized residuals are calculated from the difference between the experimental and calculated wavenumbers divided by the experimental standard deviations as given in the Appendix.

4. DISCUSSION

The (8,8) band of the BaI $C^2\Pi - X^2\Sigma^+$ transition has been rotationally analyzed by a weighted nonlinear least-squares fitting procedure. The final fit is good; the parameters are all well determined and no trends are observed in the residuals. The variance of the weighted least-squares fit is 0.582 so that the experimental wavenumbers are reproduced within their expected experimental errors. (If the weights used in the fit were, on average, the reciprocal of one experimental standard deviation, the variance would be 1.0). The molecular constants determined from the least-squares fit (see Table I) are a minimum set of parameters that reproduce the experimental transition wavenumbers. The number of figures quoted for the rotational constants, B' and B'', and the centrifugal distortion constants, D' and D'', is more than would be expected from their standard deviations because the differences between B' and B'', and D' and D'' is determined more precisely than their absolute values (*21*). The number of figures quoted is needed to reproduce the calculated wavenumbers given in the Appendix. Since the residuals from the least-squares fit show no systematic trends (see Fig. 5), we conclude that there are no major frequency perturbations affecting these transitions.

The choice of which molecular constants from the standard $^2\Pi - ^2\Sigma^+$ Hamiltonian are included in the final least-squares fit was made with the intention of obtaining a good fit to the data within the accuracy of the experiment. In particular, we comment on the Λ-doubling constant, q', which has been omitted from the fit.

The Λ-doubling constant, q'_v, is defined for a general vibrational level, v, as

$$q'_v = 2 \sum_{n'v'} \frac{\langle nvJ | B(r) L_+ | n'v'J \rangle^2}{E_{nvJ} - E_{n'v'J}}, \tag{1}$$

where the sum is over all perturbing electronic states, n', and their vibrational levels, v' (*20*). Separating the vibrational and electronic matrix elements according to the Born–Oppenheimer approximation gives

$$\langle nvJ | B(r) L_+ | n'v'J \rangle = \langle vJ | B(r) | v'J \rangle \langle n | L_+ | n' \rangle. \tag{2}$$

By neglecting the centrifugal distortion, q'_v is taken to be independent of J. Hence,

$$\langle vJ | B(r) | v'J \rangle = \langle v | B(r) | v' \rangle \tag{3}$$

and

$$E_{nvJ} - E_{n'v'J} = E_{nv} - E_{n'v'}. \tag{4}$$

This gives

$$q'_v = 2 \sum_{n'} \langle n | L_+ | n' \rangle^2 \sum_{v'} \frac{\langle v | B(r) | v' \rangle \langle v' | B(r) | v \rangle}{E_{nv} - E_{n'v'}}. \tag{5}$$

Further assumptions are necessary to enable us to estimate q'_v. First, we use the unique perturber approximation in which only one electronic Σ state is assumed to be perturbing the state. Second, we replace the energy denominator by an effective energy denominator that is independent of v'. The equation for q'_v then reduces to

$$q'_v = \frac{2\langle v|B^2(r)|v\rangle\langle n|L_+|n'\rangle^2}{E_n - E_{n'}}. \tag{6}$$

The nearest known Σ state to the $C^2\Pi$ state is the $D^2\Sigma^+$ state which has a band origin at 25 774 cm^{-1}; $E_n - E_{n'}$ is therefore close to 7600 cm^{-1} (*8*). $\langle n|L_+|n'\rangle$ is taken to be $l(l+1)$ where l is approximated by unity. We also make the approximation

$$\langle v|r^{-4}|v\rangle = \langle v|r^{-2}|v\rangle^2. \tag{7}$$

Then, for B'_8 equal to 0.026 cm^{-1}, we have the estimate q'_8 equals -3×10^{-7} cm^{-1}. However, the unique perturber approximation is not valid, since there are at least four $^2\Sigma^+$ states (X, B, D, and E) interacting with the $C^2\Pi$ state to cause the Λ doubling. This is therefore an order of magnitude estimate. The sign of q'_8 cannot be predicted since the perturbing states lie both above ($D^2\Sigma^+$ and $E^2\Sigma^+$) and below ($B^2\Sigma^+$ and $X^2\Sigma^+$) the $C^2\Pi$ state. A value of q'_8 of approximately $\pm 3 \times 10^{-7}$ cm^{-1} has very little effect on the transition wavenumbers. Thus, we conclude that q'_8 is too small to be determined from the present line positions measured. Similarly, rough estimates of the H'', H', and γ''_D constants suggest that their effects on the transitions measured would be too small to be observed.

The molecular constants given in Table I reproduce the experimental transition wavenumbers very well. However, most of the data is limited to 6 of the 12 possible rotational branches and there is a strong bias in favor of the $C^2\Pi_{1/2}$–$X^2\Sigma^+$ subband. Despite these problems we have a definite J'' assignment for all transitions measured. This has permitted a spectroscopic study of the dynamics of the beam–gas reaction, Ba + HI → BaI ($v'' = 8$) + H (*13*), and will allow additional studies under crossed-beam conditions.

APPENDIX

TABLE AI

Rotational and Branch Assignment, Experimental Wavenumbers, Calculated Wavenumbers, Standard Deviations, and Normalized Residuals for all Rotational Transitions used in the Least-Squares Fit.

Branch	J"	Experimental wavenumber (cm-1)	Calculated wavenumber (cm-1)	Experimental standard deviation(cm-1)	Normalized residual
P11	50.5	17855.9790	17855.9846	0.0050	-1.12
	54.5	17855.8250	17855.8392	0.0050	-2.84
R12	49.5	17859.0750	17859.0765	0.0050	-0.30
	53.5	17859.1860	17859.1757	0.0050	2.07
P12	190.5	17841.9378	17841.9394	0.0022	-0.71
	189.5	17842.0240	17842.0259	0.0022	-0.88
	188.5	17842.1094	17842.1125	0.0022	-1.41
	187.5	17842.1945	17842.1991	0.0022	-2.09
	186.5	17842.2804	17842.2857	0.0022	-2.41
	185.5	17842.3739	17842.3723	0.0019	0.82
	184.5	17842.4613	17842.4590	0.0019	1.22
	183.5	17842.5515	17842.5456	0.0019	3.06
	182.5	17842.6379	17842.6323	0.0019	2.92
	181.5	17842.7216	17842.7189	0.0019	1.38
	180.5	17842.8150	17842.8056	0.0030	3.13
	179.5	17842.8971	17842.8923	0.0019	2.49
	178.5	17842.9801	17842.9790	0.0019	0.58
	177.5	17843.0675	17843.0657	0.0019	0.95
	176.5	17843.1532	17843.1524	0.0019	0.43
	175.5	17843.2362	17843.2391	0.0022	-1.31
	173.5	17843.4180	17843.4125	0.0018	3.07
	172.5	17843.5049	17843.4992	0.0018	3.18
	171.5	17843.5894	17843.5859	0.0018	1.96
	170.5	17843.6749	17843.6726	0.0018	1.30
	169.5	17843.7616	17843.7593	0.0018	1.30
	168.5	17843.8482	17843.8459	0.0018	1.25
	167.5	17843.9339	17843.9326	0.0018	0.71
	166.5	17844.0187	17844.0193	0.0018	-0.33
	165.5	17844.1053	17844.1059	0.0018	-0.36
	164.5	17844.1911	17844.1926	0.0018	-0.83
	163.5	17844.2804	17844.2792	0.0018	0.65
	162.5	17844.3656	17844.3659	0.0018	-0.14
	161.5	17844.4520	17844.4525	0.0018	-0.26
	160.5	17844.5388	17844.5391	0.0018	-0.15
	159.5	17844.6236	17844.6256	0.0018	-1.14
	158.5	17844.7108	17844.7122	0.0018	-0.78
	157.5	17844.7960	17844.7988	0.0018	-1.53
	156.5	17844.8842	17844.8853	0.0018	-0.60
	155.5	17844.9693	17844.9718	0.0018	-1.38
	154.5	17845.0571	17845.0583	0.0018	-0.65
	153.5	17845.1420	17845.1447	0.0018	-1.52
	152.5	17845.2343	17845.2312	0.0018	1.74
	151.5	17845.3212	17845.3176	0.0018	2.01
	150.5	17845.4076	17845.4040	0.0018	2.02
	149.5	17845.4922	17845.4903	0.0018	1.04
	148.5	17845.5795	17845.5767	0.0018	1.58
	147.5	17845.6660	17845.6630	0.0018	1.69
	146.5	17845.7540	17845.7492	0.0018	2.64
	145.5	17845.8402	17845.8355	0.0025	1.89
	144.5	17845.9263	17845.9217	0.0025	1.84
	143.5	17846.0115	17846.0079	0.0025	1.45
	142.5	17846.0988	17846.0940	0.0025	1.91
	141.5	17846.1824	17846.1801	0.0035	0.65
	140.5	17846.2682	17846.2662	0.0035	0.57
	139.5	17846.3545	17846.3522	0.0035	0.64

TABLE AI—*Continued*

Branch	J"	Experimental wavenumber (cm-1)	Calculated wavenumber (cm-1)	Experimental standard deviation(cm-1)	Normalized residual
	138.5	17846.4393	17846.4382	0.0035	0.30
	137.5	17846.5259	17846.5242	0.0035	0.48
	136.5	17846.6112	17846.6101	0.0035	0.31
	135.5	17846.6969	17846.6960	0.0035	0.25
	134.5	17846.7832	17846.7819	0.0035	0.38
	133.5	17846.8686	17846.8677	0.0035	0.27
	132.5	17846.9530	17846.9534	0.0035	-0.12
	131.5	17847.0399	17847.0391	0.0035	0.22
	127.5	17847.3787	17847.3815	0.0040	-0.70
	126.5	17847.4654	17847.4670	0.0040	-0.39
	125.5	17847.5538	17847.5524	0.0040	0.35
	124.5	17847.6424	17847.6378	0.0040	1.16
	123.5	17847.7286	17847.7231	0.0040	1.38
	122.5	17847.8115	17847.8084	0.0040	0.78
	121.5	17847.8961	17847.8936	0.0040	0.63
	120.5	17847.9813	17847.9787	0.0040	0.64
	119.5	17848.0648	17848.0639	0.0040	0.24
	118.5	17848.1467	17848.1489	0.0040	-0.55
	117.5	17848.2316	17848.2339	0.0040	-0.57
	115.5	17848.4076	17848.4037	0.0040	0.97
	114.5	17848.4950	17848.4885	0.0040	1.62
	113.5	17848.5740	17848.5733	0.0040	0.18
	112.5	17848.6566	17848.6580	0.0040	-0.35
	111.5	17848.7394	17848.7426	0.0040	-0.81
	110.5	17848.8176	17848.8272	0.0040	-2.40
	109.5	17848.9102	17848.9117	0.0040	-0.38
	108.5	17848.9978	17848.9962	0.0040	0.41
	107.5	17849.0826	17849.0806	0.0040	0.51
	106.5	17849.1629	17849.1649	0.0040	-0.49
	105.5	17849.2514	17849.2491	0.0040	0.57
	103.5	17849.4181	17849.4174	0.0021	0.31
	102.5	17849.4999	17849.5015	0.0021	-0.75
	101.5	17849.5810	17849.5855	0.0028	-1.58
	100.5	17849.6685	17849.6694	0.0021	-0.41
	99.5	17849.7536	17849.7532	0.0021	0.18
	98.5	17849.8360	17849.8370	0.0021	-0.46
	97.5	17849.9218	17849.9207	0.0021	0.53
	96.5	17850.0044	17850.0043	0.0021	0.05
	95.5	17850.0852	17850.0878	0.0021	-1.25
	94.5	17850.1701	17850.1713	0.0021	-0.57
	93.5	17850.2551	17850.2547	0.0021	0.18
	92.5	17850.3372	17850.3380	0.0015	-0.54
	91.5	17850.4233	17850.4213	0.0018	1.12
	90.5	17850.5044	17850.5045	0.0018	-0.03
	89.5	17850.5887	17850.5875	0.0018	0.64
	88.5	17850.6716	17850.6706	0.0018	0.58
	87.5	17850.7553	17850.7535	0.0018	1.00
	86.5	17850.8376	17850.8363	0.0018	0.69
	85.5	17850.9203	17850.9191	0.0018	0.65
	84.5	17851.0036	17851.0018	0.0018	0.99
	83.5	17851.0832	17851.0844	0.0015	-0.84
	82.5	17851.1660	17851.1670	0.0015	-0.66
	81.5	17851.2488	17851.2494	0.0015	-0.42
	80.5	17851.3270	17851.3318	0.0025	-1.91
	79.5	17851.4105	17851.4140	0.0025	-1.42
	78.5	17851.4917	17851.4962	0.0025	-1.82
	77.5	17851.5743	17851.5784	0.0025	-1.62
	76.5	17851.6558	17851.6604	0.0025	-1.83
	75.5	17851.7367	17851.7423	0.0025	-2.25
	74.5	17851.8183	17851.8242	0.0025	-2.35
	73.5	17851.9007	17851.9059	0.0025	-2.09
	72.5	17851.9867	17851.9876	0.0013	-0.71

TABLE AI—*Continued*

Branch	J"	Experimental wavenumber (cm-1)	Calculated wavenumber (cm-1)	Experimental standard deviation(cm-1)	Normalized residual
	71.5	17852.0693	17852.0692	0.0013	0.09
	70.5	17852.1505	17852.1507	0.0013	-0.13
	69.5	17852.2320	17852.2321	0.0013	-0.06
	68.5	17852.3138	17852.3134	0.0013	0.30
	67.5	17852.3950	17852.3946	0.0013	0.28
	66.5	17852.4756	17852.4758	0.0013	-0.12
	65.5	17852.5567	17852.5568	0.0013	-0.08
	64.5	17852.6378	17852.6378	0.0013	0.04
	63.5	17852.7190	17852.7186	0.0013	0.29
	62.5	17852.7984	17852.7994	0.0013	-0.72
	61.5	17852.8793	17852.8800	0.0013	-0.55
	60.5	17852.9599	17852.9606	0.0018	-0.40
	59.5	17853.0423	17853.0411	0.0018	0.67
	58.5	17853.1223	17853.1215	0.0018	0.46
	57.5	17853.2036	17853.2018	0.0018	1.02
	56.5	17853.2826	17853.2820	0.0018	0.36
	55.5	17853.3624	17853.3620	0.0017	0.21
	54.5	17853.4421	17853.4420	0.0018	0.03
	53.5	17853.5216	17853.5219	0.0017	-0.20
	52.5	17853.6005	17853.6017	0.0018	-0.69
	51.5	17853.6790	17853.6815	0.0017	-1.45
	50.5	17853.7604	17853.7611	0.0018	-0.36
	49.5	17853.8376	17853.8406	0.0017	-1.75
	47.5	17854.0007	17853.9993	0.0018	0.80
	46.5	17854.0798	17854.0785	0.0018	0.74
	45.5	17854.1579	17854.1576	0.0018	0.18
	44.5	17854.2368	17854.2366	0.0018	0.13
	43.5	17854.3175	17854.3155	0.0018	1.13
	42.5	17854.3953	17854.3943	0.0018	0.57
	41.5	17854.4748	17854.4730	0.0018	1.02
	40.5	17854.5528	17854.5516	0.0018	0.69
	39.5	17854.6313	17854.6300	0.0018	0.70
	38.5	17854.7114	17854.7084	0.0040	0.74
	37.5	17854.7885	17854.7867	0.0030	0.60
	36.5	17854.8674	17854.8649	0.0030	0.84
Q12	186.5	17850.7503	17850.7511	0.0020	-0.42
	185.5	17850.7925	17850.7930	0.0020	-0.26
	184.5	17850.8346	17850.8349	0.0025	-0.13
	183.5	17850.8761	17850.8768	0.0020	-0.35
	182.5	17850.9182	17850.9187	0.0020	-0.25
	181.5	17850.9599	17850.9606	0.0020	-0.34
	180.5	17851.0019	17851.0025	0.0020	-0.29
	179.5	17851.0439	17851.0444	0.0020	-0.23
	178.5	17851.0867	17851.0862	0.0020	0.23
	177.5	17851.1278	17851.1281	0.0020	-0.16
	176.5	17851.1696	17851.1700	0.0020	-0.20
	175.5	17851.2116	17851.2119	0.0020	-0.13
	174.5	17851.2541	17851.2537	0.0025	0.16
	173.5	17851.2948	17851.2956	0.0020	-0.38
	172.5	17851.3380	17851.3374	0.0020	0.31
	171.5	17851.3788	17851.3792	0.0020	-0.20
	170.5	17851.4231	17851.4210	0.0025	0.83
	169.5	17851.4620	17851.4628	0.0020	-0.40
	168.5	17851.5048	17851.5046	0.0025	0.09
	167.5	17851.5452	17851.5463	0.0020	-0.57
	166.5	17851.5877	17851.5881	0.0025	-0.16
	165.5	17851.6290	17851.6298	0.0020	-0.41
	164.5	17851.6711	17851.6715	0.0025	-0.17
	162.5	17851.7524	17851.7549	0.0020	-1.23
	161.5	17851.7935	17851.7965	0.0020	-1.50

TABLE AI—*Continued*

Branch	J"	Experimental wavenumber (cm-1)	Calculated wavenumber (cm-1)	Experimental standard deviation(cm-1)	Normalized residual
	160.5	17851.8354	17851.8381	0.0020	-1.36
	159.5	17851.8775	17851.8797	0.0020	-1.10
	158.5	17851.9187	17851.9213	0.0020	-1.28
	157.5	17851.9605	17851.9628	0.0020	-1.15
	156.5	17852.0033	17852.0043	0.0020	-0.50
	155.5	17852.0432	17852.0458	0.0020	-1.29
	154.5	17852.0846	17852.0872	0.0020	-1.32
	153.5	17852.1255	17852.1286	0.0020	-1.57
	152.5	17852.1682	17852.1700	0.0020	-0.92
	151.5	17852.2085	17852.2114	0.0020	-1.44
	150.5	17852.2511	17852.2527	0.0020	-0.80
	149.5	17852.2915	17852.2940	0.0020	-1.24
	148.5	17852.3335	17852.3352	0.0020	-0.86
	147.5	17852.3737	17852.3764	0.0020	-1.37
	146.5	17852.4149	17852.4176	0.0020	-1.35
	145.5	17852.4563	17852.4587	0.0025	-0.97
	144.5	17852.4981	17852.4998	0.0025	-0.69
	143.5	17852.5396	17852.5409	0.0025	-0.51
	142.5	17852.5804	17852.5819	0.0025	-0.59
	141.5	17852.6209	17852.6228	0.0025	-0.78
	140.5	17852.6607	17852.6638	0.0025	-1.23
	137.5	17852.7857	17852.7863	0.0025	-0.22
	136.5	17852.8266	17852.8270	0.0025	-0.16
	135.5	17852.8674	17852.8677	0.0025	-0.11
	134.5	17852.9074	17852.9083	0.0025	-0.37
	132.5	17852.9887	17852.9894	0.0025	-0.30
	131.5	17853.0291	17853.0299	0.0025	-0.33
	130.5	17853.0692	17853.0704	0.0025	-0.46
	129.5	17853.1105	17853.1107	0.0025	-0.10
	128.5	17853.1495	17853.1511	0.0025	-0.63
	127.5	17853.1898	17853.1913	0.0025	-0.61
	126.5	17853.2296	17853.2315	0.0025	-0.78
	125.5	17853.2701	17853.2717	0.0025	-0.64
	124.5	17853.3103	17853.3118	0.0025	-0.60
	123.5	17853.3512	17853.3518	0.0025	-0.26
	122.5	17853.3906	17853.3918	0.0025	-0.49
	121.5	17853.4311	17853.4317	0.0025	-0.26
	120.5	17853.4708	17853.4716	0.0025	-0.32
	119.5	17853.5105	17853.5114	0.0025	-0.36
	118.5	17853.5506	17853.5511	0.0025	-0.21
	117.5	17853.5900	17853.5908	0.0025	-0.32
	116.5	17853.6306	17853.6304	0.0025	0.08
	112.5	17853.7876	17853.7882	0.0020	-0.29
	111.5	17853.8264	17853.8275	0.0020	-0.53
	110.5	17853.8659	17853.8667	0.0020	-0.38
	109.5	17853.9050	17853.9058	0.0020	-0.40
	108.5	17853.9437	17853.9449	0.0020	-0.58
	107.5	17853.9829	17853.9839	0.0020	-0.48
	106.5	17854.0221	17854.0228	0.0020	-0.34
	105.5	17854.0604	17854.0616	0.0020	-0.62
	104.5	17854.0998	17854.1004	0.0020	-0.31
	103.5	17854.1387	17854.1391	0.0016	-0.27
	102.5	17854.1769	17854.1777	0.0016	-0.54
	101.5	17854.2165	17854.2163	0.0016	0.13
	100.5	17854.2539	17854.2548	0.0016	-0.56
	99.5	17854.2927	17854.2932	0.0014	-0.34
	98.5	17854.3303	17854.3315	0.0014	-0.85
	97.5	17854.3691	17854.3698	0.0014	-0.46
	96.5	17854.4066	17854.4079	0.0014	-0.93
	95.5	17854.4458	17854.4460	0.0014	-0.15

TABLE AI—*Continued*

Branch	J"	Experimental wavenumber (cm-1)	Calculated wavenumber (cm-1)	Experimental standard deviation(cm-1)	Normalized residual
	94.5	17854.4837	17854.4840	0.0014	-0.23
	93.5	17854.5223	17854.5219	0.0014	0.25
	92.5	17854.5598	17854.5598	0.0014	0.00
	91.5	17854.5975	17854.5976	0.0014	-0.04
	90.5	17854.6361	17854.6352	0.0014	0.60
	89.5	17854.6721	17854.6728	0.0014	-0.53
	88.5	17854.7098	17854.7104	0.0014	-0.40
	87.5	17854.7479	17854.7478	0.0020	0.05
	86.5	17854.7846	17854.7851	0.0020	-0.27
	85.5	17854.8217	17854.8224	0.0020	-0.36
	84.5	17854.8589	17854.8596	0.0020	-0.34
	83.5	17854.8956	17854.8967	0.0020	-0.54
	82.5	17854.9335	17854.9337	0.0020	-0.09
	81.5	17854.9705	17854.9706	0.0020	-0.05
	80.5	17855.0073	17855.0074	0.0016	-0.08
	79.5	17855.0441	17855.0442	0.0016	-0.05
	78.5	17855.0800	17855.0808	0.0025	-0.33
	77.5	17855.1174	17855.1174	0.0025	0.01
	76.5	17855.1534	17855.1539	0.0025	-0.18
	75.5	17855.1895	17855.1902	0.0025	-0.29
	74.5	17855.2269	17855.2265	0.0025	0.15
	73.5	17855.2634	17855.2627	0.0025	0.27
	72.5	17855.2991	17855.2988	0.0025	0.11
	71.5	17855.3347	17855.3348	0.0025	-0.05
	70.5	17855.3709	17855.3708	0.0025	0.06
	69.5	17855.4061	17855.4066	0.0017	-0.29
	68.5	17855.4413	17855.4423	0.0017	-0.61
	67.5	17855.4775	17855.4779	0.0017	-0.27
	66.5	17855.5132	17855.5135	0.0017	-0.17
	65.5	17855.5489	17855.5489	0.0017	-0.01
	64.5	17855.5834	17855.5843	0.0017	-0.53
	63.5	17855.6186	17855.6195	0.0017	-0.56
	62.5	17855.6534	17855.6547	0.0017	-0.77
	61.5	17855.6896	17855.6897	0.0017	-0.08
	60.5	17855.7244	17855.7247	0.0017	-0.18
	59.5	17855.7595	17855.7595	0.0017	-0.03
	58.5	17855.7950	17855.7943	0.0017	0.42
	57.5	17855.8285	17855.8290	0.0013	-0.35
	56.5	17855.8637	17855.8635	0.0013	0.12
	55.5	17855.8970	17855.8980	0.0013	-0.77
	54.5	17855.9325	17855.9324	0.0013	0.11
	53.5	17855.9664	17855.9666	0.0015	-0.14
	52.5	17856.0018	17856.0008	0.0016	0.64
	51.5	17856.0343	17856.0348	0.0015	-0.35
	50.5	17856.0690	17856.0688	0.0016	0.13
	49.5	17856.1026	17856.1026	0.0015	-0.03
	48.5	17856.1370	17856.1364	0.0016	0.38
	47.5	17856.1703	17856.1700	0.0016	0.16
	46.5	17856.2044	17856.2036	0.0016	0.51
	45.5	17856.2373	17856.2370	0.0016	0.17
	44.5	17856.2700	17856.2704	0.0016	-0.23
	43.5	17856.3045	17856.3036	0.0016	0.57
	42.5	17856.3360	17856.3367	0.0016	-0.46
	41.5	17856.3704	17856.3697	0.0023	0.28
	40.5	17856.4029	17856.4027	0.0023	0.10
	39.5	17856.4364	17856.4355	0.0023	0.40
	38.5	17856.4686	17856.4682	0.0023	0.18
	37.5	17856.5013	17856.5008	0.0023	0.22
	36.5	17856.5343	17856.5333	0.0023	0.45
	35.5	17856.5656	17856.5657	0.0023	-0.03

TABLE AI—*Continued*

Branch	J"	Experimental wavenumber (cm-1)	Calculated wavenumber (cm-1)	Experimental standard deviation(cm-1)	Normalized residual
	34.5	17856.5978	17856.5979	0.0023	-0.06
	33.5	17856.6300	17856.6301	0.0023	-0.05
	32.5	17856.6621	17856.6622	0.0023	-0.03
	31.5	17856.6956	17856.6941	0.0023	0.64
	30.5	17856.7266	17856.7260	0.0023	0.27
	29.5	17856.7582	17856.7577	0.0023	0.21
Q11	13.5	17858.0427	17858.0444	0.0035	-0.49
	14.5	17858.0757	17858.0711	0.0035	1.31
	15.5	17858.0990	17858.0977	0.0035	0.36
	16.5	17858.1241	17858.1242	0.0035	-0.03
	17.5	17858.1596	17858.1506	0.0035	2.58
	18.5	17858.1771	17858.1768	0.0035	0.07
	19.5	17858.2030	17858.2030	0.0018	0.00
	20.5	17858.2313	17858.2290	0.0018	1.28
	21.5	17858.2553	17858.2550	0.0018	0.19
	22.5	17858.2820	17858.2808	0.0013	0.97
	23.5	17858.3076	17858.3065	0.0013	0.89
	24.5	17858.3328	17858.3321	0.0013	0.58
	25.5	17858.3592	17858.3575	0.0013	1.31
	26.5	17858.3839	17858.3829	0.0013	0.79
	27.5	17858.4090	17858.4081	0.0013	0.67
	28.5	17858.4336	17858.4333	0.0013	0.25
	29.5	17858.4593	17858.4583	0.0018	0.55
	30.5	17858.4840	17858.4832	0.0018	0.43
	31.5	17858.5091	17858.5080	0.0018	0.59
	32.5	17858.5323	17858.5327	0.0013	-0.34
	33.5	17858.5581	17858.5573	0.0013	0.62
	34.5	17858.5815	17858.5818	0.0013	-0.22
	35.5	17858.6064	17858.6061	0.0013	0.20
	36.5	17858.6306	17858.6304	0.0013	0.16
	37.5	17858.6553	17858.6545	0.0013	0.60
	38.5	17858.6784	17858.6786	0.0013	-0.13
	39.5	17858.7026	17858.7025	0.0013	0.09
	40.5	17858.7261	17858.7263	0.0013	-0.16
	41.5	17858.7504	17858.7500	0.0013	0.31
	42.5	17858.7723	17858.7736	0.0018	-0.72
	43.5	17858.7963	17858.7971	0.0018	-0.43
	44.5	17858.8193	17858.8205	0.0013	-0.90
	45.5	17858.8428	17858.8437	0.0013	-0.72
	46.5	17858.8659	17858.8669	0.0013	-0.76
	47.5	17858.8892	17858.8899	0.0013	-0.57
	48.5	17858.9117	17858.9129	0.0013	-0.91
	49.5	17858.9341	17858.9357	0.0013	-1.25
	50.5	17858.9560	17858.9584	0.0012	-1.96
	51.5	17858.9806	17858.9810	0.0013	-0.34
	52.5	17859.0023	17859.0035	0.0013	-0.98
	53.5	17859.0258	17859.0260	0.0013	-0.12
	54.5	17859.0477	17859.0482	0.0012	-0.45
	55.5	17859.0698	17859.0704	0.0013	-0.50
	56.5	17859.0914	17859.0925	0.0013	-0.89
	57.5	17859.1140	17859.1145	0.0013	-0.40
	58.5	17859.1356	17859.1364	0.0013	-0.62
	59.5	17859.1573	17859.1582	0.0013	-0.67
	60.5	17859.1794	17859.1798	0.0013	-0.33
	61.5	17859.2015	17859.2014	0.0013	0.09
	62.5	17859.2229	17859.2228	0.0013	0.05
	63.5	17859.2444	17859.2442	0.0013	0.16
	64.5	17859.2661	17859.2654	0.0013	0.52
	65.5	17859.2860	17859.2866	0.0013	-0.46
	66.5	17859.3077	17859.3076	0.0013	0.05

TABLE AI—*Continued*

Branch	J"	Experimental wavenumber (cm-1)	Calculated wavenumber (cm-1)	Experimental standard deviation(cm-1)	Normalized residual
	67.5	17859.3289	17859.3286	0.0013	0.25
	68.5	17859.3495	17859.3494	0.0013	0.06
	69.5	17859.3698	17859.3702	0.0013	-0.28
	70.5	17859.3914	17859.3908	0.0013	0.47
	71.5	17859.4111	17859.4113	0.0013	-0.19
	72.5	17859.4312	17859.4318	0.0013	-0.45
	73.5	17859.4519	17859.4521	0.0013	-0.17
	74.5	17859.4721	17859.4724	0.0018	-0.14
	75.5	17859.4913	17859.4925	0.0013	-0.94
	76.5	17859.5123	17859.5125	0.0013	-0.18
	77.5	17859.5322	17859.5325	0.0013	-0.22
	78.5	17859.5527	17859.5523	0.0013	0.30
	79.5	17859.5721	17859.5721	0.0013	0.03
	80.5	17859.5921	17859.5917	0.0013	0.30
	81.5	17859.6119	17859.6113	0.0013	0.49
	82.5	17859.6316	17859.6307	0.0013	0.68
	83.5	17859.6503	17859.6501	0.0013	0.16
	84.5	17859.6703	17859.6694	0.0013	0.74
	85.5	17859.6890	17859.6885	0.0016	0.28
	86.5	17859.7079	17859.7076	0.0014	0.20
	87.5	17859.7270	17859.7266	0.0014	0.28
	88.5	17859.7446	17859.7455	0.0015	-0.58
	89.5	17859.7627	17859.7643	0.0015	-1.03
	90.5	17859.7817	17859.7830	0.0015	-0.84
	91.5	17859.8020	17859.8016	0.0015	0.25
	92.5	17859.8180	17859.8201	0.0015	-1.39
	93.5	17859.8377	17859.8386	0.0015	-0.56
	94.5	17859.8565	17859.8569	0.0018	-0.23
	95.5	17859.8735	17859.8752	0.0018	-0.93
	96.5	17859.8922	17859.8933	0.0018	-0.63
	97.5	17859.9110	17859.9114	0.0018	-0.23
	98.5	17859.9289	17859.9294	0.0015	-0.33
	99.5	17859.9460	17859.9473	0.0015	-0.84
	100.5	17859.9647	17859.9651	0.0015	-0.27
	101.5	17859.9841	17859.9828	0.0015	0.81
	102.5	17860.0002	17860.0005	0.0015	-0.19
	103.5	17860.0183	17860.0181	0.0015	0.16
	104.5	17860.0360	17860.0355	0.0019	0.25
	105.5	17860.0537	17860.0529	0.0019	0.41
	106.5	17860.0696	17860.0702	0.0019	-0.32
	107.5	17860.0875	17860.0874	0.0019	0.03
	108.5	17860.1066	17860.1046	0.0019	1.05
	109.5	17860.1206	17860.1216	0.0019	-0.55
	110.5	17860.1380	17860.1386	0.0019	-0.33
	111.5	17860.1544	17860.1555	0.0014	-0.83
	112.5	17860.1715	17860.1723	0.0014	-0.62
	113.5	17860.1871	17860.1891	0.0015	-1.33
	114.5	17860.2043	17860.2058	0.0014	-1.07
	115.5	17860.2213	17860.2223	0.0014	-0.77
	116.5	17860.2382	17860.2388	0.0015	-0.44
	117.5	17860.2547	17860.2553	0.0016	-0.36
	118.5	17860.2706	17860.2716	0.0015	-0.71
	119.5	17860.2900	17860.2879	0.0017	1.26
	120.5	17860.3035	17860.3041	0.0015	-0.43
	121.5	17860.3200	17860.3203	0.0015	-0.18
	122.5	17860.3362	17860.3363	0.0018	-0.07
	123.5	17860.3531	17860.3523	0.0016	0.49
	124.5	17860.3670	17860.3682	0.0016	-0.77
	125.5	17860.3831	17860.3841	0.0016	-0.62
	126.5	17860.3996	17860.3999	0.0018	-0.15

TABLE AI—*Continued*

Branch	J"	Experimental wavenumber (cm-1)	Calculated wavenumber (cm-1)	Experimental standard deviation(cm-1)	Normalized residual
	127.5	17860.4167	17860.4156	0.0020	0.58
	128.5	17860.4297	17860.4312	0.0015	-0.98
	129.5	17860.4458	17860.4468	0.0015	-0.64
	130.5	17860.4617	17860.4623	0.0015	-0.38
	131.5	17860.4775	17860.4777	0.0015	-0.15
	132.5	17860.4925	17860.4931	0.0015	-0.39
	133.5	17860.5091	17860.5084	0.0018	0.39
	134.5	17860.5230	17860.5237	0.0018	-0.37
	135.5	17860.5389	17860.5388	0.0015	0.03
	136.5	17860.5521	17860.5540	0.0015	-1.21
	137.5	17860.5686	17860.5690	0.0016	-0.26
	138.5	17860.5852	17860.5840	0.0016	0.73
	139.5	17860.5983	17860.5990	0.0016	-0.41
	140.5	17860.6122	17860.6138	0.0016	-1.02
	141.5	17860.6276	17860.6287	0.0019	-0.57
	142.5	17860.6428	17860.6434	0.0019	-0.33
	143.5	17860.6577	17860.6581	0.0019	-0.23
	144.5	17860.6717	17860.6728	0.0019	-0.57
	145.5	17860.6864	17860.6874	0.0019	-0.51
	146.5	17860.7009	17860.7019	0.0019	-0.54
	147.5	17860.7175	17860.7164	0.0019	0.56
	148.5	17860.7305	17860.7309	0.0019	-0.19
	149.5	17860.7448	17860.7452	0.0019	-0.23
	150.5	17860.7590	17860.7596	0.0019	-0.30
	151.5	17860.7741	17860.7739	0.0019	0.12
	152.5	17860.7881	17860.7881	0.0019	0.00
	153.5	17860.8024	17860.8023	0.0019	0.06
	154.5	17860.8165	17860.8164	0.0015	0.05
	155.5	17860.8325	17860.8305	0.0030	0.66
	156.5	17860.8458	17860.8446	0.0030	0.41
	157.5	17860.8585	17860.8586	0.0015	-0.05
	158.5	17860.8731	17860.8725	0.0015	0.37
	159.5	17860.8860	17860.8865	0.0015	-0.30
	160.5	17860.9002	17860.9003	0.0015	-0.09
	161.5	17860.9134	17860.9142	0.0015	-0.51
	162.5	17860.9287	17860.9280	0.0015	0.47
	163.5	17860.9430	17860.9417	0.0015	0.83
	164.5	17860.9553	17860.9555	0.0015	-0.11
	165.5	17860.9683	17860.9691	0.0015	-0.56
	166.5	17860.9819	17860.9828	0.0015	-0.59
	167.5	17860.9968	17860.9964	0.0015	0.26
	168.5	17861.0138	17861.0100	0.0040	0.95
	169.5	17861.0266	17861.0235	0.0040	0.77
	170.5	17861.0356	17861.0371	0.0019	-0.78
	171.5	17861.0499	17861.0505	0.0016	-0.40
	172.5	17861.0653	17861.0640	0.0023	0.56
	173.5	17861.0812	17861.0774	0.0040	0.94
	174.5	17861.0923	17861.0908	0.0040	0.37
	175.5	17861.1037	17861.1042	0.0021	-0.23
	176.5	17861.1190	17861.1175	0.0028	0.52
	177.5	17861.1296	17861.1309	0.0040	-0.32
	179.5	17861.1554	17861.1574	0.0025	-0.82
	180.5	17861.1710	17861.1707	0.0031	0.10
	181.5	17861.1886	17861.1839	0.0050	0.93
	183.5	17861.2085	17861.2103	0.0025	-0.73
	184.5	17861.2233	17861.2235	0.0025	-0.09
	185.5	17861.2355	17861.2367	0.0022	-0.53
	186.5	17861.2492	17861.2498	0.0022	-0.28
	187.5	17861.2599	17861.2630	0.0025	-1.22
	188.5	17861.2786	17861.2761	0.0025	1.01

TABLE AI—*Continued*

Branch	J"	Experimental wavenumber (cm-1)	Calculated wavenumber (cm-1)	Experimental standard deviation(cm-1)	Normalized residual
	189.5	17861.2880	17861.2892	0.0022	-0.53
	190.5	17861.3018	17861.3023	0.0022	-0.22
	191.5	17861.3142	17861.3154	0.0025	-0.47
	192.5	17861.3272	17861.3285	0.0025	-0.50
	193.5	17861.3393	17861.3415	0.0025	-0.89
	194.5	17861.3548	17861.3546	0.0031	0.06
	195.5	17861.3655	17861.3677	0.0022	-0.97
	196.5	17861.3795	17861.3807	0.0040	-0.31
	197.5	17861.3944	17861.3938	0.0040	0.15
	200.5	17861.4302	17861.4329	0.0040	-0.69
	201.5	17861.4431	17861.4460	0.0040	-0.73
	204.5	17861.4832	17861.4852	0.0040	-0.50
	205.5	17861.4978	17861.4983	0.0025	-0.19
	207.5	17861.5225	17861.5245	0.0040	-0.49
	210.5	17861.5651	17861.5638	0.0040	0.32
	211.5	17861.5749	17861.5770	0.0040	-0.52
	213.5	17861.6003	17861.6033	0.0040	-0.75
	235.5	17861.8990	17861.9002	0.0040	-0.29
	236.5	17861.9130	17861.9141	0.0040	-0.28
	237.5	17861.9281	17861.9281	0.0040	0.00
	238.5	17861.9414	17861.9421	0.0040	-0.18
	239.5	17861.9547	17861.9562	0.0050	-0.30
	240.5	17861.9698	17861.9703	0.0050	-0.11
	241.5	17861.9827	17861.9845	0.0040	-0.46
	242.5	17861.9961	17861.9988	0.0040	-0.67
	243.5	17862.0112	17862.0131	0.0040	-0.47
	251.5	17862.1258	17862.1298	0.0040	-0.99
	252.5	17862.1435	17862.1447	0.0040	-0.29
	253.5	17862.1578	17862.1596	0.0040	-0.45
	254.5	17862.1750	17862.1746	0.0050	0.07
	255.5	17862.1885	17862.1898	0.0040	-0.32
	256.5	17862.2056	17862.2049	0.0040	0.16
	257.5	17862.2210	17862.2202	0.0040	0.20
	258.5	17862.2349	17862.2356	0.0050	-0.13
	259.5	17862.2521	17862.2510	0.0040	0.28
	260.5	17862.2642	17862.2665	0.0040	-0.58
	261.5	17862.2827	17862.2821	0.0040	0.15
	262.5	17862.3022	17862.2978	0.0040	1.10
	263.5	17862.3151	17862.3136	0.0050	0.31
	265.5	17862.3434	17862.3454	0.0040	-0.49
	268.5	17862.3825	17862.3938	0.0050	-2.26
	269.5	17862.4087	17862.4101	0.0040	-0.35
	270.5	17862.4240	17862.4265	0.0040	-0.64
	271.5	17862.4404	17862.4431	0.0040	-0.67
R11	47.5	17861.1067	17861.1064	0.0018	0.19
	48.5	17861.1764	17861.1749	0.0018	0.81
	49.5	17861.2440	17861.2434	0.0018	0.32
	50.5	17861.3143	17861.3118	0.0017	1.47
	51.5	17861.3810	17861.3801	0.0018	0.52
	52.5	17861.4487	17861.4482	0.0018	0.27
	53.5	17861.5159	17861.5163	0.0018	-0.20
	54.5	17861.5842	17861.5842	0.0017	0.00
	55.5	17861.6527	17861.6520	0.0018	0.38
	56.5	17861.7194	17861.7197	0.0018	-0.19
	57.5	17861.7875	17861.7873	0.0018	0.09
	58.5	17861.8542	17861.8548	0.0018	-0.36
	59.5	17861.9223	17861.9222	0.0018	0.04
	60.5	17861.9891	17861.9895	0.0018	-0.23
	61.5	17862.0567	17862.0567	0.0018	0.01
	62.5	17862.1235	17862.1238	0.0035	-0.07

TABLE AI—*Continued*

Branch	J"	Experimental wavenumber (cm-1)	Calculated wavenumber (cm-1)	Experimental standard deviation(cm-1)	Normalized residual
	63.5	17862.1903	17862.1907	0.0035	-0.12
	64.5	17862.2575	17862.2576	0.0035	-0.02
	65.5	17862.3243	17862.3243	0.0035	0.00
	66.5	17862.3909	17862.3909	0.0035	-0.01
	67.5	17862.4574	17862.4575	0.0035	-0.02
	68.5	17862.5236	17862.5239	0.0035	-0.09
	69.5	17862.5899	17862.5902	0.0035	-0.09
	70.5	17862.6550	17862.6564	0.0035	-0.41
	71.5	17862.7215	17862.7226	0.0035	-0.30
	72.5	17862.7896	17862.7886	0.0016	0.65
	73.5	17862.8553	17862.8545	0.0016	0.52
	74.5	17862.9203	17862.9203	0.0016	0.02
	75.5	17862.9870	17862.9860	0.0016	0.64
	76.5	17863.0526	17863.0516	0.0018	0.58
	77.5	17863.1188	17863.1171	0.0018	0.97
	78.5	17863.1840	17863.1824	0.0018	0.87
	79.5	17863.2492	17863.2477	0.0018	0.82
	80.5	17863.3147	17863.3129	0.0018	0.99
	81.5	17863.3795	17863.3780	0.0018	0.83
	82.5	17863.4440	17863.4430	0.0018	0.57
	83.5	17863.5084	17863.5079	0.0018	0.30
	84.5	17863.5732	17863.5726	0.0018	0.31
	85.5	17863.6380	17863.6373	0.0018	0.37
	86.5	17863.7031	17863.7019	0.0018	0.66
	87.5	17863.7675	17863.7664	0.0018	0.61
	88.5	17863.8319	17863.8308	0.0018	0.62
	89.5	17863.8955	17863.8951	0.0018	0.23
	90.5	17863.9602	17863.9593	0.0018	0.51
	91.5	17864.0249	17864.0234	0.0018	0.85
	92.5	17864.0886	17864.0874	0.0018	0.68
	93.5	17864.1519	17864.1513	0.0018	0.35
	94.5	17864.2155	17864.2151	0.0018	0.23
	95.5	17864.2789	17864.2788	0.0018	0.06
	96.5	17864.3427	17864.3424	0.0018	0.16
	97.5	17864.4055	17864.4059	0.0018	-0.25
	98.5	17864.4695	17864.4694	0.0018	0.07
	99.5	17864.5320	17864.5327	0.0013	-0.56
	100.5	17864.5954	17864.5960	0.0018	-0.31
	101.5	17864.6584	17864.6591	0.0018	-0.40
	102.5	17864.7215	17864.7222	0.0018	-0.37
	103.5	17864.7846	17864.7851	0.0025	-0.22
	104.5	17864.8485	17864.8480	0.0025	0.19
	105.5	17864.9098	17864.9108	0.0025	-0.41
	106.5	17864.9714	17864.9735	0.0025	-0.85
	110.5	17865.2274	17865.2234	0.0050	0.79
	111.5	17865.2869	17865.2857	0.0050	0.24
	112.5	17865.3460	17865.3479	0.0050	-0.38
	113.5	17865.4106	17865.4100	0.0050	0.12
	114.5	17865.4744	17865.4720	0.0050	0.48
	115.5	17865.5325	17865.5339	0.0050	-0.28
	116.5	17865.6003	17865.5958	0.0050	0.91
	117.5	17865.6564	17865.6575	0.0050	-0.22
	118.5	17865.7226	17865.7192	0.0050	0.68
	119.5	17865.7786	17865.7808	0.0050	-0.44
	120.5	17865.8438	17865.8423	0.0050	0.30
	121.5	17865.9063	17865.9037	0.0026	1.00
	122.5	17865.9652	17865.9651	0.0022	0.06
	123.5	17866.0264	17866.0263	0.0022	0.02
	124.5	17866.0876	17866.0875	0.0022	0.02
	125.5	17866.1505	17866.1487	0.0022	0.82

TABLE AI—*Continued*

Branch	J"	Experimental wavenumber (cm-1)	Calculated wavenumber (cm-1)	Experimental standard deviation(cm-1)	Normalized residual
	126.5	17866.2108	17866.2097	0.0025	0.44
	127.5	17866.2709	17866.2707	0.0013	0.18
	128.5	17866.3311	17866.3316	0.0013	-0.36
	129.5	17866.3920	17866.3924	0.0013	-0.29
	130.5	17866.4535	17866.4531	0.0013	0.31
	131.5	17866.5138	17866.5138	0.0013	0.02
	132.5	17866.5750	17866.5744	0.0013	0.50
	133.5	17866.6354	17866.6349	0.0013	0.41
	134.5	17866.6956	17866.6953	0.0013	0.21
	135.5	17866.7564	17866.7557	0.0013	0.55
	136.5	17866.8168	17866.8160	0.0010	0.76
	137.5	17866.8761	17866.8763	0.0013	-0.12
	138.5	17866.9370	17866.9364	0.0010	0.56
	139.5	17866.9967	17866.9965	0.0010	0.17
	140.5	17867.0570	17867.0566	0.0010	0.43
	141.5	17867.1169	17867.1165	0.0010	0.36
	142.5	17867.1775	17867.1764	0.0013	0.84
	143.5	17867.2371	17867.2363	0.0013	0.66
	144.5	17867.2966	17867.2960	0.0013	0.44
	145.5	17867.3565	17867.3557	0.0013	0.59
	146.5	17867.4161	17867.4154	0.0013	0.55
	147.5	17867.4758	17867.4750	0.0013	0.64
	148.5	17867.5357	17867.5345	0.0013	0.94
	149.5	17867.5951	17867.5940	0.0013	0.89
	150.5	17867.6540	17867.6534	0.0013	0.49
	151.5	17867.7137	17867.7127	0.0013	0.76
	152.5	17867.7712	17867.7720	0.0018	-0.45
	153.5	17867.8304	17867.8313	0.0018	-0.47
	157.5	17868.0676	17868.0676	0.0025	-0.01
	158.5	17868.1269	17868.1266	0.0018	0.17
	159.5	17868.1860	17868.1855	0.0018	0.27
	160.5	17868.2449	17868.2444	0.0018	0.29
	161.5	17868.3041	17868.3032	0.0018	0.51
	162.5	17868.3621	17868.3619	0.0018	0.09
	163.5	17868.4214	17868.4207	0.0018	0.41
	164.5	17868.4802	17868.4793	0.0018	0.49
	165.5	17868.5378	17868.5379	0.0018	-0.08
	166.5	17868.5973	17868.5965	0.0018	0.43
	167.5	17868.6562	17868.6551	0.0018	0.64
	168.5	17868.7148	17868.7135	0.0018	0.70
	169.5	17868.7722	17868.7720	0.0018	0.12
	170.5	17868.8308	17868.8304	0.0018	0.23
	171.5	17868.8896	17868.8888	0.0018	0.47
	172.5	17868.9480	17868.9471	0.0018	0.51
	173.5	17869.0069	17869.0054	0.0018	0.86
	174.5	17869.0615	17869.0636	0.0018	-1.17
	175.5	17869.1209	17869.1218	0.0018	-0.51
	176.5	17869.1785	17869.1800	0.0018	-0.83
	177.5	17869.2369	17869.2381	0.0018	-0.68
	178.5	17869.2951	17869.2962	0.0018	-0.63
	179.5	17869.3531	17869.3543	0.0018	-0.67
	180.5	17869.4128	17869.4124	0.0018	0.25
	181.5	17869.4698	17869.4704	0.0018	-0.31
	182.5	17869.5291	17869.5283	0.0018	0.42
	183.5	17869.5845	17869.5863	0.0018	-1.00
	184.5	17869.6419	17869.6442	0.0018	-1.29
	185.5	17869.7011	17869.7021	0.0018	-0.56
	186.5	17869.7589	17869.7600	0.0018	-0.60
	187.5	17869.8161	17869.8178	0.0018	-0.96
	188.5	17869.8738	17869.8757	0.0018	-1.03

TABLE AI—*Continued*

Branch	J"	Experimental wavenumber (cm-1)	Calculated wavenumber (cm-1)	Experimental standard deviation(cm-1)	Normalized residual
	189.5	17869.9304	17869.9335	0.0018	-1.70
	190.5	17869.9889	17869.9912	0.0018	-1.30
	191.5	17870.0493	17870.0490	0.0018	0.17
	192.5	17870.1068	17870.1067	0.0018	0.03
	193.5	17870.1662	17870.1645	0.0018	0.97
	194.5	17870.2215	17870.2222	0.0018	-0.37
	195.5	17870.2800	17870.2799	0.0018	0.08
	196.5	17870.3378	17870.3375	0.0018	0.15
	197.5	17870.3942	17870.3952	0.0018	-0.55
	198.5	17870.4517	17870.4528	0.0018	-0.63
	199.5	17870.5100	17870.5105	0.0018	-0.26
	200.5	17870.5682	17870.5681	0.0018	0.06
	201.5	17870.6260	17870.6257	0.0018	0.16
	202.5	17870.6840	17870.6833	0.0018	0.38
	203.5	17870.7433	17870.7409	0.0018	1.32
	204.5	17870.8015	17870.7985	0.0018	1.66
	205.5	17870.8567	17870.8561	0.0018	0.33
	206.5	17870.9149	17870.9137	0.0018	0.67
	207.5	17870.9693	17870.9713	0.0018	-1.09
R21	49.5	18618.4750	18618.4663	0.0050	1.74
	117.5	18623.1220	18623.1217	0.0026	0.12
	118.5	18623.1870	18623.1870	0.0026	0.00
	119.5	18623.2525	18623.2522	0.0026	0.11
	120.5	18623.3183	18623.3174	0.0026	0.36
	121.5	18623.3824	18623.3824	0.0026	-0.01
	122.5	18623.4464	18623.4474	0.0026	-0.40
	123.5	18623.5111	18623.5123	0.0026	-0.48
	124.5	18623.5771	18623.5772	0.0026	-0.03
	125.5	18623.6408	18623.6419	0.0026	-0.44
	126.5	18623.7056	18623.7066	0.0026	-0.40
	127.5	18623.7688	18623.7713	0.0026	-0.94
	128.5	18623.8343	18623.8358	0.0026	-0.57
	129.5	18623.9011	18623.9003	0.0021	0.40
	130.5	18623.9656	18623.9647	0.0017	0.55
	131.5	18624.0301	18624.0290	0.0017	0.65
	132.5	18624.0943	18624.0932	0.0017	0.62
	133.5	18624.1603	18624.1574	0.0023	1.24
	134.5	18624.2231	18624.2215	0.0023	0.68
	135.5	18624.2867	18624.2856	0.0023	0.49
	136.5	18624.3507	18624.3496	0.0023	0.50
	137.5	18624.4149	18624.4135	0.0023	0.62
	138.5	18624.4792	18624.4773	0.0023	0.82
	139.5	18624.5428	18624.5411	0.0023	0.74
	140.5	18624.6050	18624.6048	0.0023	0.09
	141.5	18624.6686	18624.6684	0.0023	0.07
	142.5	18624.7313	18624.7320	0.0014	-0.51
	143.5	18624.7951	18624.7955	0.0014	-0.31
	144.5	18624.8590	18624.8590	0.0014	0.00
	145.5	18624.9224	18624.9224	0.0018	0.00
	146.5	18624.9853	18624.9857	0.0018	-0.24
	147.5	18625.0463	18625.0490	0.0018	-1.51
	148.5	18625.1104	18625.1122	0.0018	-1.02
	149.5	18625.1737	18625.1754	0.0018	-0.94
	150.5	18625.2364	18625.2385	0.0018	-1.16
	151.5	18625.3009	18625.3015	0.0018	-0.35
	152.5	18625.3653	18625.3645	0.0018	0.43
	153.5	18625.4256	18625.4275	0.0018	-1.03
	154.5	18625.4873	18625.4903	0.0018	-1.69
	155.5	18625.5525	18625.5532	0.0012	-0.56
	156.5	18625.6153	18625.6159	0.0012	-0.54

TABLE AI—*Continued*

Branch	J"	Experimental wavenumber (cm-1)	Calculated wavenumber (cm-1)	Experimental standard deviation(cm-1)	Normalized residual
	157.5	18625.6781	18625.6787	0.0012	-0.47
	158.5	18625.7418	18625.7413	0.0016	0.29
	159.5	18625.8051	18625.8040	0.0016	0.72
	160.5	18625.8658	18625.8665	0.0016	-0.46
	161.5	18625.9282	18625.9291	0.0016	-0.54
	162.5	18625.9908	18625.9915	0.0016	-0.47
	163.5	18626.0542	18626.0540	0.0016	0.14
	164.5	18626.1162	18626.1164	0.0016	-0.10
	165.5	18626.1763	18626.1787	0.0016	-1.51
	166.5	18626.2395	18626.2410	0.0016	-0.94
	167.5	18626.3023	18626.3033	0.0013	-0.72
	168.5	18626.3648	18626.3655	0.0013	-0.51
	169.5	18626.4271	18626.4276	0.0013	-0.41
	170.5	18626.4897	18626.4898	0.0015	-0.05
	171.5	18626.5524	18626.5519	0.0024	0.22
	172.5	18626.6165	18626.6139	0.0024	1.07
	173.5	18626.6750	18626.6759	0.0024	-0.39
	174.5	18626.7369	18626.7379	0.0024	-0.43
	175.5	18626.7997	18626.7999	0.0024	-0.07
	176.5	18626.8609	18626.8618	0.0024	-0.37
	177.5	18626.9228	18626.9237	0.0024	-0.36
	178.5	18626.9832	18626.9855	0.0024	-0.96
	179.5	18627.0449	18627.0473	0.0024	-1.01
	180.5	18627.1081	18627.1091	0.0014	-0.71
	181.5	18627.1706	18627.1709	0.0014	-0.19
	182.5	18627.2326	18627.2326	0.0014	0.00
	183.5	18627.2941	18627.2943	0.0014	-0.14
	184.5	18627.3571	18627.3560	0.0018	0.62
	185.5	18627.4194	18627.4176	0.0018	0.99
	186.5	18627.4790	18627.4793	0.0018	-0.14
	187.5	18627.5398	18627.5409	0.0018	-0.58
	188.5	18627.6016	18627.6024	0.0018	-0.46
	189.5	18627.6628	18627.6640	0.0018	-0.66
	190.5	18627.7258	18627.7255	0.0018	0.15
	191.5	18627.7861	18627.7870	0.0018	-0.53
	192.5	18627.8467	18627.8485	0.0018	-1.03
	193.5	18627.9079	18627.9100	0.0015	-1.38
	194.5	18627.9703	18627.9715	0.0015	-0.78
	195.5	18628.0321	18628.0330	0.0015	-0.55
	196.5	18628.0939	18628.0944	0.0015	-0.32
	197.5	18628.1564	18628.1558	0.0030	0.19
	198.5	18628.2167	18628.2172	0.0030	-0.18
	202.5	18628.4627	18628.4628	0.0018	-0.06
	203.5	18628.5249	18628.5242	0.0018	0.40
	204.5	18628.5857	18628.5855	0.0018	0.08
	205.5	18628.6474	18628.6469	0.0018	0.27
	206.5	18628.7099	18628.7083	0.0018	0.90
	207.5	18628.7677	18628.7696	0.0018	-1.08
	208.5	18628.8314	18628.8310	0.0018	0.22
	209.5	18628.8938	18628.8924	0.0018	0.80
	210.5	18628.9565	18628.9537	0.0018	1.54
	211.5	18629.0167	18629.0151	0.0018	0.89
	212.5	18629.0772	18629.0765	0.0018	0.40
	213.5	18629.1393	18629.1379	0.0018	0.80
	214.5	18629.2015	18629.1992	0.0018	1.25
	215.5	18629.2627	18629.2606	0.0015	1.34
	216.5	18629.3247	18629.3220	0.0015	1.72
	217.5	18629.3876	18629.3835	0.0015	2.69
	218.5	18629.4472	18629.4449	0.0030	0.77
	219.5	18629.5095	18629.5063	0.0030	1.06

TABLE AI—*Continued*

Branch	J"	Experimental wavenumber (cm-1)	Calculated wavenumber (cm-1)	Experimental standard deviation(cm-1)	Normalized residual
	220.5	18629.5665	18629.5678	0.0030	-0.42
	221.5	18629.6297	18629.6292	0.0030	0.15
	222.5	18629.6902	18629.6907	0.0030	-0.18
	223.5	18629.7525	18629.7522	0.0030	0.09
	224.5	18629.8164	18629.8138	0.0030	0.88
P22	50.5	18610.6570	18610.6507	0.0050	1.26
	52.5	18610.4930	18610.4851	0.0050	1.57
	119.5	18604.7460	18604.7470	0.0020	-0.48
	120.5	18604.6614	18604.6590	0.0020	1.20
	121.5	18604.5714	18604.5710	0.0020	0.21
	122.5	18604.4835	18604.4829	0.0020	0.29
	123.5	18604.3965	18604.3948	0.0020	0.84
	124.5	18604.3045	18604.3067	0.0020	-1.08
	125.5	18604.2202	18604.2184	0.0020	0.88
	126.5	18604.1346	18604.1302	0.0020	2.20
	127.5	18604.0431	18604.0419	0.0020	0.60
	128.5	18603.9533	18603.9535	0.0018	-0.14
	129.5	18603.8671	18603.8652	0.0018	1.07
	130.5	18603.7761	18603.7767	0.0042	-0.15
	131.5	18603.6872	18603.6883	0.0042	-0.25
	132.5	18603.6035	18603.5997	0.0042	0.89
	133.5	18603.5146	18603.5112	0.0042	0.81
	134.5	18603.4236	18603.4226	0.0042	0.24
	137.5	18603.1552	18603.1566	0.0032	-0.43
	138.5	18603.0661	18603.0679	0.0032	-0.55
	139.5	18602.9765	18602.9791	0.0032	-0.80
	140.5	18602.8881	18602.8903	0.0032	-0.68
	141.5	18602.7995	18602.8014	0.0032	-0.60
	142.5	18602.7107	18602.7126	0.0032	-0.58
	143.5	18602.6247	18602.6236	0.0029	0.36
	144.5	18602.5366	18602.5347	0.0029	0.64
	145.5	18602.4473	18602.4458	0.0029	0.52
	146.5	18602.3579	18602.3568	0.0029	0.38
	147.5	18602.2686	18602.2678	0.0029	0.29
	148.5	18602.1808	18602.1787	0.0029	0.71
	149.5	18602.0907	18602.0896	0.0029	0.36
	150.5	18602.0017	18602.0006	0.0029	0.39
	151.5	18601.9128	18601.9114	0.0029	0.46
	152.5	18601.8280	18601.8223	0.0075	0.76
	153.5	18601.7373	18601.7332	0.0075	0.55
	154.5	18601.6483	18601.6440	0.0075	0.57
	155.5	18601.5598	18601.5548	0.0075	0.67
	156.5	18601.4707	18601.4656	0.0075	0.68
	157.5	18601.3801	18601.3764	0.0075	0.50
	158.5	18601.2924	18601.2871	0.0075	0.70
	159.5	18601.2024	18601.1979	0.0075	0.60
	160.5	18601.1125	18601.1086	0.0075	0.52
	161.5	18601.0238	18601.0193	0.0075	0.59
	162.5	18600.9340	18600.9301	0.0075	0.53
	163.5	18600.8449	18600.8408	0.0075	0.55
	164.5	18600.7559	18600.7514	0.0075	0.59
	165.5	18600.6654	18600.6621	0.0075	0.43
	166.5	18600.5758	18600.5728	0.0075	0.40
	167.5	18600.4858	18600.4835	0.0075	0.31
	168.5	18600.3961	18600.3942	0.0075	0.26
	169.5	18600.3109	18600.3048	0.0075	0.81
	170.5	18600.2163	18600.2155	0.0032	0.25
	171.5	18600.1263	18600.1262	0.0032	0.04
	172.5	18600.0364	18600.0368	0.0032	-0.14
	173.5	18599.9484	18599.9475	0.0032	0.28

TABLE AI—*Continued*

Branch	J"	Experimental wavenumber (cm-1)	Calculated wavenumber (cm-1)	Experimental standard deviation(cm-1)	Normalized residual
	174.5	18599.8586	18599.8582	0.0032	0.13
	175.5	18599.7684	18599.7689	0.0032	-0.15
	176.5	18599.6789	18599.6796	0.0032	-0.21
	177.5	18599.5904	18599.5902	0.0035	0.04
	178.5	18599.4991	18599.5009	0.0035	-0.53
	179.5	18599.4097	18599.4117	0.0035	-0.56
	180.5	18599.3199	18599.3224	0.0035	-0.71
	181.5	18599.2328	18599.2331	0.0035	-0.09
	182.5	18599.1429	18599.1438	0.0035	-0.27
	183.5	18599.0535	18599.0546	0.0035	-0.32
	184.5	18598.9627	18598.9654	0.0035	-0.76
	185.5	18598.8750	18598.8762	0.0035	-0.33
	186.5	18598.7853	18598.7870	0.0035	-0.48
	187.5	18598.6961	18598.6978	0.0035	-0.48
	188.5	18598.6078	18598.6086	0.0035	-0.24
	189.5	18598.5188	18598.5195	0.0035	-0.20
	190.5	18598.4292	18598.4304	0.0035	-0.34
	191.5	18598.3399	18598.3413	0.0035	-0.40
	192.5	18598.2517	18598.2523	0.0035	-0.16
	193.5	18598.1635	18598.1632	0.0035	0.08
	194.5	18598.0740	18598.0742	0.0035	-0.06
	195.5	18597.9833	18597.9852	0.0035	-0.56
	196.5	18597.8957	18597.8963	0.0035	-0.17
	197.5	18597.8069	18597.8074	0.0035	-0.14
	198.5	18597.7177	18597.7185	0.0024	-0.34
	199.5	18597.6282	18597.6297	0.0024	-0.61
	200.5	18597.5393	18597.5409	0.0024	-0.65
	201.5	18597.4514	18597.4521	0.0024	-0.28
	202.5	18597.3637	18597.3633	0.0024	0.15
	203.5	18597.2737	18597.2747	0.0027	-0.36
	204.5	18597.1838	18597.1860	0.0027	-0.83
	205.5	18597.0939	18597.0974	0.0045	-0.78
	206.5	18597.0088	18597.0088	0.0045	-0.01
	207.5	18596.9208	18596.9203	0.0045	0.11
	210.5	18596.6502	18596.6550	0.0045	-1.08
	211.5	18596.5635	18596.5667	0.0045	-0.71
	212.5	18596.4773	18596.4784	0.0045	-0.25
	213.5	18596.3889	18596.3902	0.0045	-0.30
	214.5	18596.2993	18596.3021	0.0045	-0.61
	215.5	18596.2103	18596.2140	0.0045	-0.81
	216.5	18596.1231	18596.1259	0.0045	-0.63
	217.5	18596.0375	18596.0379	0.0045	-0.10
	218.5	18595.9539	18595.9500	0.0045	0.87
	219.5	18595.8673	18595.8621	0.0045	1.15
	220.5	18595.7749	18595.7743	0.0045	0.12
	221.5	18595.6853	18595.6866	0.0045	-0.29
	222.5	18595.6007	18595.5989	0.0045	0.39
	223.5	18595.5168	18595.5113	0.0045	1.21
P21	51.5	18613.1700	18613.1712	0.0050	-0.25
Q21	49.5	18615.8330	18615.8253	0.0050	1.54
	51.5	18615.8720	18615.8644	0.0050	1.52
Q22	50.5	18613.2890	18613.2916	0.0050	-0.53
R22	48.5	18615.9430	18615.9411	0.0050	0.39
	50.5	18615.9890	18615.9848	0.0050	0.83

ACKNOWLEDGMENTS

The authors thank A. A. Tsekouras, P. H. Vaccaro, and D. Zhao for useful discussions. CAL thanks the Lindemann Trust and NATO for a postdoctoral fellowship. This work is supported under NSF CHE 89-21198.

RECEIVED: November 29, 1990

REFERENCES

1. M. A. JOHNSON, C. NODA, J. S. MCKILLOP, AND R. N. ZARE, *Canad. J. Phys.* **62,** 1467–1473 (1984).
2. O. H. WALTERS AND S. BARRATT, *Proc. R. Soc. London A* **118,** 120–137 (1928).
3. P. MESNAGE, *Ann. Phys.* **12,** 5–9 (1939).
4. M. M. PATEL AND N. R. SHAH, *Ind. J. Pure Appl. Phys.* **8,** 681–682 (1970).
5. R. S. BRADFORD, JR., C. R. JONES, L. A. SOUTHALL, AND H. P. BROIDA, *J. Chem. Phys.* **62,** 2060–2064 (1975).
6. W. M. L. FERNANDO, M. DOUAY, AND P. F. BERNATH, *J. Mol. Spectrosc.,* **144,** 344–351 (1990).
7. M. L. P. RAO, D. V. K. RAO, P. T. RAO, AND P. S. MURTY, *Fizika* **9,** 25–29 (1977).
8. M. M. PATEL, private communication, 1975.
9. M. A. JOHNSON, J. ALLISON, AND R. N. ZARE, *J. Chem. Phys.* **85,** 5723–5732 (1986).
10. W. E. ERNST, J. KANDLER, C. NODA, J. S. MCKILLOP, AND R. N. ZARE, *J. Chem. Phys.* **85,** 3735–3743 (1986).
11. M. A. JOHNSON AND R. N. ZARE, *J. Chem. Phys.* **82,** 4449–4459 (1985); M. A. JOHNSON, C. W. WEBSTER, AND R. N. ZARE, *J. Chem. Phys.* **75,** 5575–5577 (1981).
12. T. TÖRRING AND K. DÖBL, *Chem. Phys. Lett.* **115,** 328–332 (1985).
13. C. NODA, J. S. MCKILLOP, M. A. JOHNSON, J. R. WALDECK, AND R. N. ZARE, *J. Chem. Phys.* **85,** 856–864 (1986).
14. P. H. VACCARO, D. ZHAO, A. A. TSEKOURAS, C. A. LEACH, W. E. ERNST, AND R. N. ZARE, *J. Chem. Phys.,* **93,** 8544–8556 (1990).
15. P. J. DAGDIGIAN, H. W. CRUSE, AND R. N. ZARE, *J. Chem. Phys.* **60,** 2330–2339 (1974).
16. G. HERZBERG, "Molecular Spectra and Molecular Structure I. Spectra of Diatomic Molecules," Van Nostrand–Reinhold, New York, 1950.
17. C. LINTON, *J. Mol. Spectrosc.* **69,** 351–364 (1978).
18. M. DULICK, P. F. BERNATH, AND R. W. FIELD, *Canad. J. Phys.* **58,** 703–712 (1980).
19. S. GERSTENKORN AND P. LUC, "Atlas du spectre d'absorption de la molécule d'iode," Centre National de la Recherche Scientifique, Paris, 1978; S. GERSTENKORN AND P. LUC, *Rev. Phys. Appl.* **14,** 791–794 (1979).
20. R. N. ZARE, A. L. SCHMELTEKOPF, W. J. HARROP, AND D. L. ALBRITTON, *J. Mol. Spectrosc.* **46,** 37–66 (1973).
21. D. L. ALBRITTON, A. L. SCHMELTEKOPF, AND R. N. ZARE, *in* "Molecular Spectroscopy: Modern Research" (K. Narahari Rao, Ed.), Vol. II, p. 1, Academic Press, New York, 1976.